JOURNAL OF CATALYSIS 134, 506–524 (1992)

Microstructural and Spectroscopic Investigations of the Supported Copper–Alumina Oxide System: Nature of Aging in Oxidizing Reaction Media

S. F. TIKHOV, V. A. SADYKOV,[1] G. N. KRYUKOVA, E. A. PAUKSHTIS, V. V. POPOVSKII, T. G. STAROSTINA, G. V. KHARLAMOV, V. F. ANUFRIENKO, V. F. POLUBOYAROV, V. A. RAZDOBAROV, N. N. BULGAKOV, AND A. V. KALINKIN

Institute of Catalysis, Siberian Branch of the USSR Academy of Sciences, Prospekt Lavrentieva 5, Novosibirsk 630090, USSR

Received June 4, 1990; revised April 2, 1991

By means of electron microscopy, infrared spectroscopy of adsorbed CO, XPS, and ESR the state of the copper oxide component of the Cu–Al–O system (CuO/γ-Al_2O_3 and bulk $CuAl_2O_4$ catalysts) has been investigated. Several types of copper–oxygen entities were detected on the catalyst surfaces: isolated ions, weak magnetic associates, two- and three-dimensional clusters, defect CuO phase. The dependence of their distribution on composition, preparation, and pretreatment conditions and their reducibility by carbon monoxide have been analyzed. The enthalpy of oxygen adsorption on copper atoms in various structures has been calculated by a semiempirical, interacting-bond method. The most reactive species are three-dimensional clusters reducing to Cu^0 by CO even at 163 K. Prolonged treatment in reaction media (CH_3OH, CH_2O, O_2 at 673–873 K) annealed extended defects in CuO particles and destroyed the clusters, forming perfect CuO particles and bulk aluminate.

INTRODUCTION

Catalysts based upon Cu–Al oxides have been used in a variety of processes in the chemical industry (*1–3*). They have been investigated by different physical methods, including IR spectroscopy (*4*), XPS (*5, 6*), SIMS (*7*), ESR (*8*), and others (*9–11*). Results for CuO/γ-Al_2O_3 are summarized by Friedman *et al.* (*9*). The most interesting data were obtained using IR spectroscopy of adsorbed molecules (CO and NO) which enabled two-dimensional (type 1) and three-dimensional (type 2) Cu–O clusters on the surface of CuO/γ-Al_2O_3, CuO/MgO systems (*12–14*) to be distinguished. However, a number of essential questions remain. Due to the presence of several types of surface species (clusters and CuO phase), there is an overlap of the absorption bands of CO adsorbed on various centers. As a result, no quantitative data concerning the relative concentration of clusters are currently available. A great deal remains to be learned about the structure of various copper–oxygen clusters on the surface of the support and their catalytic significance. Transmission electron microscopy (TEM) has not been used in previous investigations even though it may be a powerful tool for the systematic research of catalyst microstructures and, as a consequence, of the nature of active centers.

Previously we reported (*15–17*) the results of an investigation of the surface active centers of pure CuO by means of TEM, IR spectroscopy, and the semiempirical quantum-chemical interacting bond method (IBM) that we use as a starting point for the analysis of the properties of active centers of the more complex Cu–Al–O system. Our efforts are devoted mainly to the investigation of the copper–alumina catalysts for environmental

[1] To whom correspondence should be addressed.

0021-9517/92 $3.00

applications. We hope to understand the nature of their active centers and to clarify the mechanism of their aging in reaction media. The results obtained should form the basis for the interpretation of catalytic properties of these samples, which will be given in a separate publication.

EXPERIMENTAL

The details of the sample preparation are described elsewhere (*18*); the most essential properties are given in Table 1.

For infrared experiments, wafers with densities of 10–30 mg/cm^2 (pressed at $\approx$100 kg/cm^2) were used. They were placed in an IR cell that allowed thermal treatment in controlled atmosphere and in vacuum. The samples were pretreated at 623 K by three subsequent procedures: (1) 1 h O_2 (150–200 Torr), 1 h vacuum (10^{-4}–10^{-5} Torr), 1 h O_2—"oxidized" samples (1 Torr = 133.3 N $\cdot$ m^{-2}); (2) 1 h O_2, 1 h vacuum—"vacuum-treated" samples; (3) 1 h O_2, 1 h vacuum, 0.5 h CO (22 Torr)—"CO-reduced" samples.

The gases (oxygen and carbon monoxide) were purified from traces of moisture and oil by passage through traps cooled with liquid nitrogen. In the case of bulk CuO, reduction by CO at 623 K was accompanied by a sharp decline in transmittance. Therefore, this oxide was treated with CO at 623 K for only 15 s. Pretreated samples were cooled to room temperature, evacuated to ca. 10^{-4} Torr, and cooled to 163 K with subsequent addition of 12–13 Torr CO. After measurement of the IR spectra in 2000–2200, 1200–1900, 3400–3480 cm^{-1} regions on a UR-20 spectrometer, the samples were warmed to 323 K and the spectra were recorded again. In typical experiments transmittance was higher than 15–20%. For a number of cases the intensities and positions of the absorption bands varied as a function of CO coverage; the coverage was changed by adsorption of subsequent doses of CO at 163 K or by evacuation at 323 K. For the systematic analysis, the decomposition of a spectral feature into its individual components has been performed as in (*19*) using a CK-12 curve synthesizer (Fig. 1). Those bonds that were clearly observed as separate maxima or shoulders under a broad range of experimental parameters were chosen as a basis. The coverage of the surface with CO adsorbed on various centers was evaluated by using these basis bands. To estimate the coverage as in (*20*), the corresponding values of the integral coefficient of absorption A_0 were used (in cm $\cdot$ μmole): for the 2120 cm^{-1} band, 8.7; for the 2130 cm^{-1} band, 10 (*21, 22*); for the 2180–2190 cm^{-1} band, 0.4 (*20*); for the 2100–2105 cm^{-1} band the value of A_0 was estimated using previous data (*23*).

ESR spectra were obtained at 77 and 300 K on a JES—3BX spectrometer. Determination of the g-factor was carried out with a $VOSO_4 \cdot 9H_2O$ standard using nomograms (*24*).

XPS spectra were recorded using an ESCA-3 spectrometer (AlKα radiation). The spectrometer was calibrated using Au $4f_{7/2}$ (binding energy (BE) = 83.8 eV) and Cu $2p_{3/2}$ (BE = 932.4 eV) bands obtained for metal foils. The resolution of the apparatus, determined as the energetic width of the Au $4f_{7/2}$ band at half-maximum (FWHM), was equal to 1.8 eV. The samples were prepared by deposition on a tungsten or nickel grid spark-welded to a tantalum holder. Preliminary sample treatment was carried out in a pretreatment chamber of the spectrometer under static conditions at the same temperatures and pressures that were used in the IR experiments. For spectral calibration the binding energy of the Al $2p$ band at 74.5 eV was used as an internal standard. The relative copper content in the surface layer was calculated by using the ratio of the areas of the Cu $2p_{3/2}$ and Al $2p$ bands. The relative factors of elemental sensitivity were experimentaly obtained previously (*25*) and in our case (Al $2p$/Cu $2p_{3/2}$) their ratio was equal to 0.014.

TEM investigations were carried out on a JEM-100CX electron microscope, with the sample prepared as described previously (*15*). The microprobe analysis was performed using "Kevex" X-ray energy dispersive spectrometer.

TABLE 1

Preparation and Some Properties of Various Catalysts

Catalyst designation	Copper content (wt% of CuO)	Content of CuO phase (wt% by XRD)	Calcination temperature (K)	Surface area (m^2/g)	Method of preparation (*18, 27*)
Cu(3.5)	3.5	—	673	180	Impregnation of γ-Al_2O_3 granules by solution of ammonium carbonate copper complex, washing out physisorbed complex by distilled water, drying at 393 K, and calcination
Cu(7)					
Initial	7.0	—	673	180	Internal part of the shell catalyst IK-12-3 (*18, 27*) obtained as Cu(3.5) without washing
Spent	7.0	2.9	673	180	Internal part of spent IK-12-3 (2 months of detoxication of CH_3OH (~2100 mg/m^3), CH_2O (~1800 mg/m^3), CO (~1 vol%) in air at 673–873 K), V.r. ~20,000 h^{-1}
Cu(20)					
Initial	20	7.0	673	180	External part (~1 mm) of IK-12-3 granules
Spent	20	7.6	673	180	External part of spent IK-12-3 granules
Cu(27)					
Initial	27	20	673	155	Impregnation of γ-Al_2O_3 by saturated solution of copper nitrate, drying, and calcination
Spent	27	12	673	117	1.5 years use under the same condition as IK-12-3
$CuAl_2O_4$	44	—	1173	12	Coprecipitation of copper and aluminum hydroxides with NaOH from nitrates solution, washing out from sodium admixtures, and calcination
CuO	100	100	673	22	Decomposition of basic copper carbonate at 673 K and washing by distilled water

RESULTS

1. TEM

The morphology and structural features of the specimens under investigation are given in Figs. 2–4 and are described below. Selected area electron diffraction patterns were used for phase identification of the particles with different morphology.

1.1. Model Systems

The result's of the detailed electron microscopic study of the bulk CuO can be found elsewhere (*15, 16*).

The Cu(3.5) specimen is morphologically homogeneous; the particles have the form of thin, elongated platelets of the γ-Al_2O_3 support. To reduce it slightly, this sample

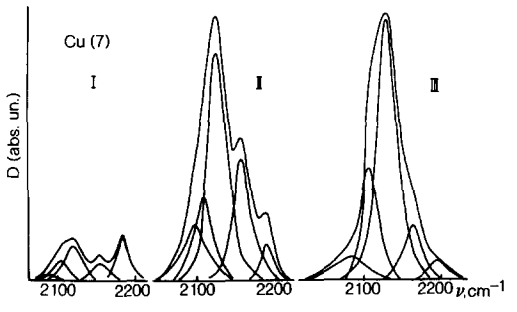

FIG. 1. Example of the decomposition of infrared spectra of adsorbed CO for the Cu(7) specimen at 163 K.

was annealed in the electron microscope under a vacuum of approximately 2×10^{-7} Torr at 623 K for 0.5 h. Small clusters on the surface of γ-Al_2O_3 particles have been observed under such experimental conditions. These clusters are shown in Fig. 2 (arrows); their mean diameter is about 60 Å. The formation of clusters during vacuum treatment may be related to the aggregation of copper ions (atoms) due to their reduction. It also seems likely that these clusters are more metallic than oxidic in nature as a result of their reaction with gaseous species in the microscope (the primary components of the residual gas are CO, CO_2, H_2O, N_2, and O_2).

The particles of the $CuAl_2O_4$ specimen have the form of platelets with clear-cut faces (see Fig. 3). The most developed faces are oriented along the (110) direction. The micrograph shows a great number of steps normal to the (110) plane. The high-resolution image of the sample clearly reveals these steps (see inset in Fig. 3). Large white dots are seen between the top and the second chains of dots representing a projection of rows of Al and Cu atoms. They could be associated with some kind of surface imperfections. However, this anomalously high contrast may also be ascribed to a charge on the surface due to polarizing effects of the incident electron beam. Another explanation for this phenomenon may stem from the loss of oxygen from the surface induced by the electron beam. This is manifested in the

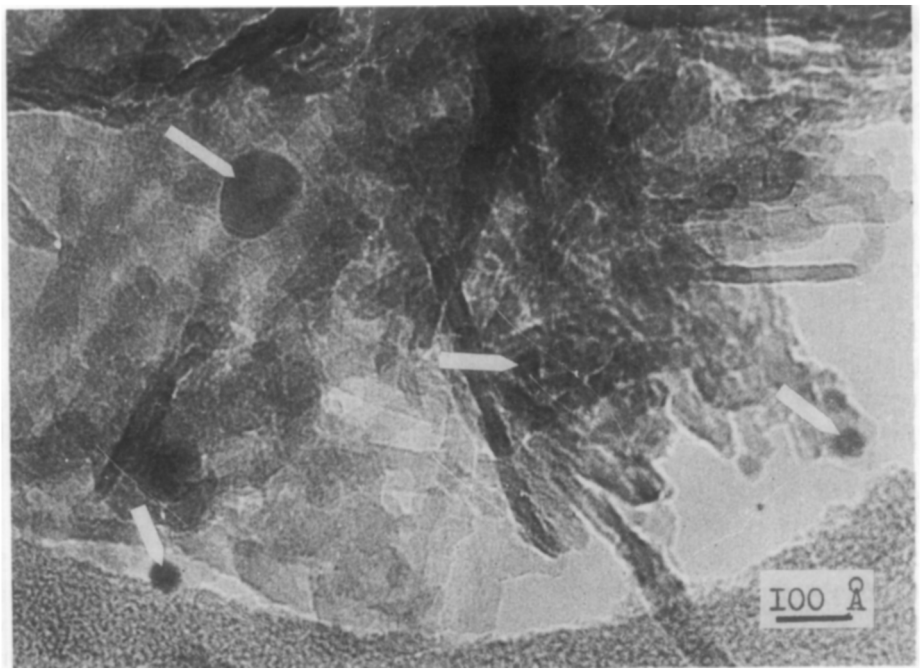

FIG. 2. Micrograph of the Cu(3.5) sample after heating at 623 K in the pretreatment chamber of the electron microscope. Cu clusters are indicated by arrows.

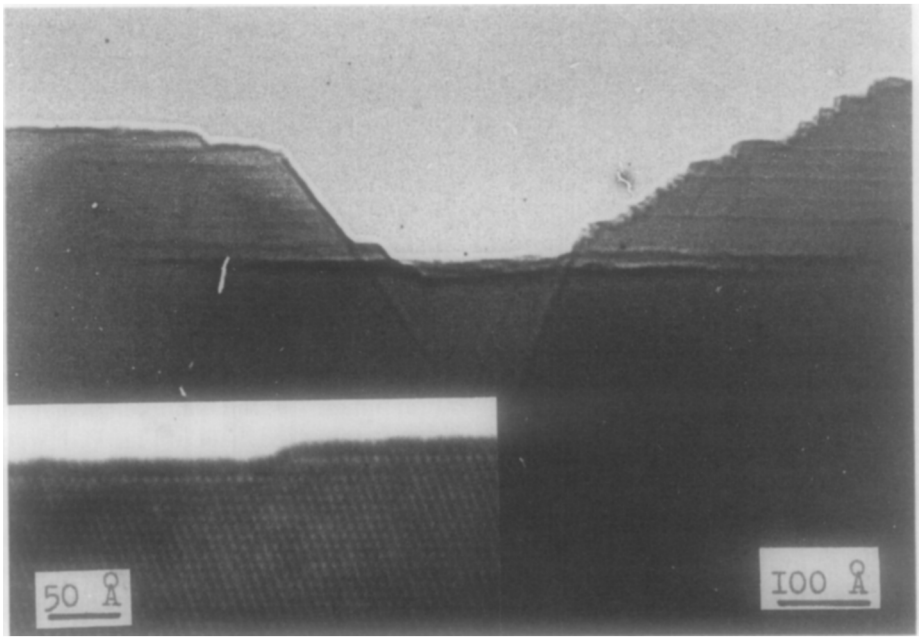

FIG. 3. Image of a $CuAl_2O_4$ particle. Inset shows a high-resolution image of a surface step.

"metallization" of the near-surface layer that has been observed in several oxides (*26*). As a result, the subsurface layer could be reconstructed.

1.2. Real Catalysts

1.2.1. Initial specimens. The morphology and phase composition of the particles are the same for all specimens of the initial catalysts. There are γ-Al_2O_3, $CuAl_2O_4$, and CuO (excluding the sample Cu(7) where no CuO phase was found). The mean diameter of the $CuAl_2O_4$ spinel particles with a morphology described above is in the range 300–400 Å. The sizes of CuO microcrystals are close in magnitude, being in the range of 0.2–0.8 μm. The structure of CuO particles is characterized by a high desnity of dislocations and polysynthetic (001) twins analogous to those reported in (*16*) (observed defects are indicated by A and B, respectively, in Fig. 4).

Electron microscopy also revealed the presence of the thick aggregates of γ-alumina particles for all fresh catalysts. previous authors (*27*) reported on the formation of CuO from such agglomerates after exposure to the electron beam in the electron microscope column. Therefore, it seems likely that the aggregates of γ-Al_2O_3 are the regions with considerable local enrichment with copper ions.

1.2.2. Spent samples. The microstructure of the spent catalysts is the same as that of fresh ones. Additionally, the regions of local copper enrichment have been destroyed, probably by a formation of thin particles of CuO and/or $CuAl_2O_4$. These CuO microcrystals possess the perfect arrangement (for the Cu(7) specimen) as well as twinned structure (for Cu(20) and Cu(27) samples).

2. XPS

The main results are given in Table 2. It seems useful to comment on the results for fresh and spent samples separately.

2.1. Initial Samples

For the oxidized state of the Cu(3.5) and Cu(7) samples, the BE of the main maxima Cu $2p_{3/2}$ is equal to 935.3–935.6 eV, which is sufficiently close to the values for bulk $CuAl_2O_4$. These values of BE, which are

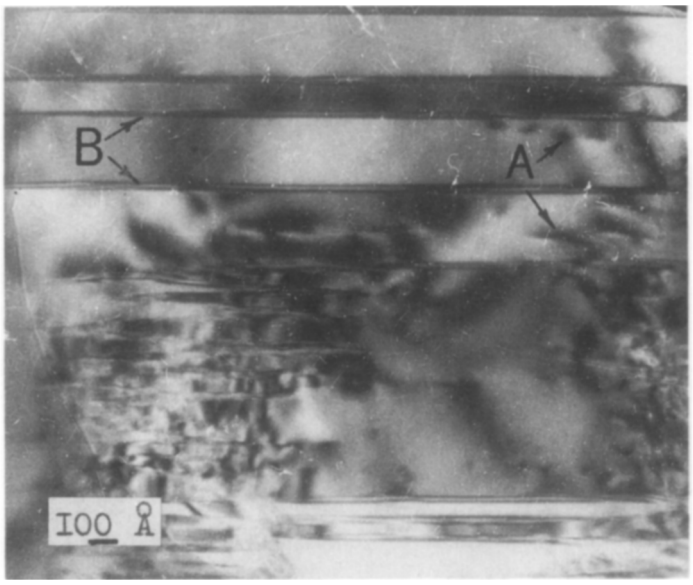

FIG. 4. Typical image of dislocations (A) and twins (B) in the CuO particle in the initial Cu(27) specimen.

somewhat higher than those for bulk CuO (*5, 6*), can be explained by coordination of copper ions by oxygen linked to highly charged Al^{3+} ions. Increased values of s/m for Cu(3.5), Cu(27), and $CuAl_2O_4$ (Table 2) can be connected with the appearance of Cu^{2+} ions in a distorted octahedral symmetry that shows satellite peaks generally stronger than those in a distorted square-planar symmetry such as in CuO (*28*). The decreased values of kinetic energy of the Cu_{LMM} Auger line by analogy with (*28, 29*) can be explained by alterations in the energy of 3*d* electrons for the surface compounds of copper or by relaxation effects. According to (*28*), this feature may be typical of copper ions diluted by diamagnetic ions (i.e., Al^{3+}, Zn^{2+}, etc.). It should be noted, however, that Auger lines in general are poorly resolved, thus often preventing detailed discussion. Moreover, for both samples, in the oxidized state the shoulder at ca. 933–933.5 eV is clearly visible, which corresponds to the Cu(+1) state. These features were explained earlier (*5, 29*) by reduction of the surface layer caused by the flux of X-ray radiation in the high-vacuum chamber of the spectrometer, leading to complete disappearance of the satellites at prolonged exposures.

Vacuum treatment of these samples leads to a shift in the BE of main maxima Cu $2p_{3/2}$ to 933.3–933.5 eV and to a considerable decrease in the satellite intensity as the result of the reduction of a predominant part of Cu^{2+} ions to the Cu^{1+} state. After CO reduction (treatment 3) of Cu(3.5) and Cu(7) the satellite completely disappeared. However, the BE of the Cu $2p_{3/2}$ band is equal to 933.1–933.2 eV, which is somewhat higher than that for Cu_2O (*5*)—932.6 eV. Low values of kinetic energy of the Auger line indicate that even after sufficiently strong reduction with CO, the predominant oxidation state of copper in the surface layer of Cu(3.5) and Cu(7) is close to Cu^{1+}. Apparently, the predominant portion of copper ions on the surface of these sample is coordinated by the oxygen of the support—γ-Al_2O_3. As a result, these ions could not be reduced under our conditions to metallic state (Cu^0) and were stabilized in the Cu^{1+} form.

For the Cu(20) sample containing the CuO

TABLE 2

XPS Parameters

Sample	Treatment 1				Treatment 2				Treatment 3			
	Cu $2p_{3/2}$ (eV)	Cu_{LMM}	Cu/Al	s/m	Cu $2p_{3/2}$ (eV)	Cu_{LMM}	Cu/Al	s/m	Cu $2p_{3/2}$ (eV)	Cu_{LMM}	Cu/Al	s/m
Cu(3.5)	935.3 ≈933^{sh}	915.5	0.015	0.55	933.3	≈914	0.012	0.08	933.2	≈914	0.014	0
Cu(7)	935.4 ≈933.5^{sh}	914.6	0.026	0.38	933.5	≈914	≈0.020	0.04	933.1	≈914	0.021	0
Cu(20)	933.9	917.4	0.071	0.44	932.8	916.5	0.044	≈0	932.4	918.7	0.030	0
Cu(27)	934.5 ≈933	915.6	0.054	0.61	932.8	≈914	0.040	0.13	933	918	0.028	0
$CuAl_2O_4$	934.8	≈916	0.090	0.89	—	—	—	—	—	—	—	—
	934.8	≈916	0.325[a]	0.90	933.7 930.1^{sh}	916 912	0.23	0.65	—	—	—	—
Cu(7) spent	935.6 ≈933.5^{sh}	—	0.024	0.41	933.5	—	0.020	0.08	934.4	—	0.020	0
Cu(20) spent	935 ≈933.5^{sh}	—	0.025	0.43	933.4	—	0.024	0.11	933	—	0.022	0
Cu(27) spent	934.3 ≈933^{sh}	916.9	0.136	0.70	932.7	≈916	0.090	0.40	—	—	—	—
$CuAl_2O_4$[b]	935.0	916.5	—	1.10	—	—	—	—	—	—	—	—
CuO	934.1	917.5	—	0.45	—	—	—	—	—	—	—	—
Cu_2O[b]	932.6	916.5	—	—	—	—	—	—	—	—	—	—
Cu[b]	932.6	918.5	—	—	—	—	—	—	—	—	—	—

Note. Cu/Al, relative copper content in the surface layer; s/m, satellite/main; sh, shoulder.

[a] After prolonged treatment in oxygen at 573 K.

[b] Strohmeier *et al.* (*5*).

phase (Table 1), XPS parameters of the main maxima Cu $2p_{3/2}$, Cu_{LMM} as well as the s/m ratio for oxidized, vacuum-treated, and reduced CO states are close to the corresponding values for CuO, Cu_2O, and Cu^0 (*5*), respectively. Moreover, the Cu(20) sample is considerably less sensitive than Cu(3.5) and Cu(7) to the flux of X-ray.

For the Cu(27) sample, the XPS parameters are close to those of Cu(20). However, the enhanced value of s/m and the reduced kinetic energy of the Cu_{LMM} line may indicate a higher concentration of the spinel $CuAl_2O_4$ in Cu(27), which is in good agreement with TEM (see above) and XRD (*27*) data.

Therefore, the properties of samples with a low concentration of active component (Cu(3.5) and Cu(7)) differ considerably from those of the supported CuO phase and bulk $CuAl_2O_4$, which is in agreement with (*5*). It should be noted that for Cu(7) and Cu(20), treatments 2 and 3 (Table 2) caused a considerable decrease in the Cu/Al ratio. This phenomenon was observed earlier (*5*) and was explained by the decrease in the dispersion of the active component after reduction.

2.2. *Spent Samples*

For the oxidized state of samples Cu(7) and Cu(20), the BE of the main maxima of the Cu $2p_{3/2}$ band is in the range 935.0–935.6 eV. In addition, there is a shoulder with lower BE, ca. 933–934 eV, which may be ascribed to the state of Cu^{2+} ions in CuO or to Cu^{1+} ions (*5*, *28*). In this case because the satellites did not change their instensity under the X-ray flux, the first explanation is more probable. The decrease in the Cu/Al ratio for spent Cu(7) and Cu(20) could be explained by the formation of sufficiently thick particles of CuO as a result of the decomposition of surface solid solution (*27*), i.e., by aggregation. The opposite trend for spent Cu(27) is probably caused by the formation of the aluminate phase accompanied by a decrease in the CuO particle thickness (*27*). After vacuum treatment the maximum is shifted to 933.4–933.5 eV. However, the degree of sample reduction within the probing depth characterized by the m/s ratio after this treatment (Table 2) is considerably lower for Cu(20) and Cu(27) spent samples than for the initial ones. A probable explanation for this is the presence of tetrahedrally coordinated Cu^{2+} ions, which are resistant to reducation. Indeed, bulk $CuAl_2O_4$, having copper ions in this coordination, demonstrates similar properties (Table 2). Moreover, after $CuAl_2O_4$ and spent Cu(27) catalyst are subjected to treatment 2, the distance between the parent peaks and the satellite decreases by 1.5–2 eV, approaching the value typical for Cu^{2+}_{td} (*28*).

After reduction by carbon monoxide (treatment 3) the maximum of the Cu $2p_{3/2}$ band remains in the region 933.0–933.4 eV, indicating incomplete reduction to Cu^0. Unfortunately, for spent samples the Cu_{LMM} Auger lines could not be reliably analyzed due to considerable broadening. Note that after treatments 2 and 3 the Cu/Al ratio for spent Cu(20) remains practically unchanged, in contrast to the behavior of the initial sample. It seems that an increase in CuO particles caused by reaction medium (*27*) occurred at the expense of easily reducible and more mobile copper–oxygen structures. The remaining part of the active component dispersed on the support is considerably more stable and less reactive. With regard to the CuO phase, either its contribution to XPS spectra is small or it is characterized by properties essentially different from those of the initial phase, with reactivity being greatly suppressed.

3. ESR

For the samples investigated, the ESR spectral parameters ($g_\parallel$ = 2.32–2.37; $g_\perp$ = 2.07–2.085; $A_\parallel$ = 127–157 Gs) correspond to Cu^{2+} ions in distorted octahedral coordination approaching a square-planar one. The fraction of copper ions detected by ESR versus copper content and the pretreatment conditions are summarized in Table 3. In some cases a considerable increase in intensity was observed after pyridine addition,

TABLE 3

ESR Data

Sample	Pretreatment	Percentage of Cu^{2+} ions by ESR	
		As received	After pyridine addition
Cu(3.5)	None	25	43
	O_2, vacuum, O_2 623 K	18	30
Cu(7)	None	5	5
	O_2, vacuum, O_2 623 K	8	8
Cu(20)	None	1.8	3.3
	O_2, vacuum, O_2 623 K	3.1	6.0
	Vacuum, 623 K	3.5[a]	7.1
Cu(27)	None	5	5
	O_2, vacuum, O_2 623 K	2.5	5.2
$CuAl_2O_4$	None	≈0.3	≈0.3
Cu(7) spent	None	0.4	0.8
Cu(20) spent	None	6.4	12.8
Cu(27) spent	None	0.05	0.1

[a] Sample kept under vacuum in sealed tube.

indicating an easy destruction of weak magnetic interactions with the formation of various pyridinates. From the data in Table 3 it can also be seen that the standard oxidative treatment before IR experiments leads to alterations in the initial state of the sample.

4. IR Spectroscopy

The CO absorption bands in IR spectra of various samples are very similar, as evident from Figs. 5 and 6; their relationship depends upon the nature of the sample and pretreatment conditions.

To discriminate the type of adsorption centers, to determine their relative concentrations, and to evaluate reactivities, an analysis of the band intensity variations for fresh samples as a function of experimental conditions and pretreatment has been carried out with the results of other methods taken into account. A sufficiently detailed description of the properties of the adsorption centers for fresh samples may facilitate an understanding of the mechanism of their aging in reaction media.

2180–2190 cm^{-1}

According to (*30*) Me^{n+}–CO complexes with ν_{CO} in this frequency region may be attributed to CO adsorbed on coordinatively unsaturated Al^{3+} ions (cf. Fig. 5 inset with spectra of CO adsorbed on γ-Al_2O_3) and Cu^{2+} ions. Indeed, centers of this type were detected for vacuum-treated bulk CuO (Fig. 6), where they can only be Cu^{2+} ions.

For oxidized bulk CuO the absence of this band means that the regular Cu^{2+} ions in square-planar coordination typical of ideal planes of this oxide cannot adsorb CO even at 163 K due to their coordinative saturation. However, this band appears for bulk CuO evacuated at high temperature and seems to be associated with the formation of coordinatively unsaturated Cu^{2+} and Cu^{1+}

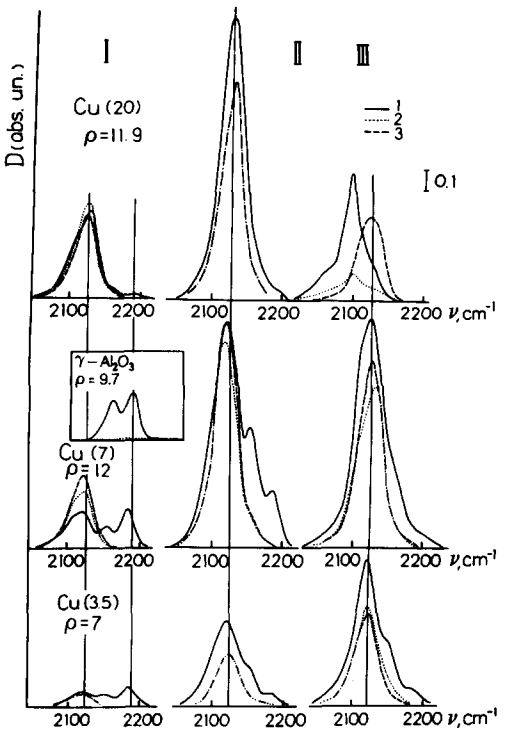

FIG. 5. Infrared spectra of CO adsorbed on Cu(3.5), Cu(7), Cu(20), and γ-Al_2O_3 samples. I, treatment 1; II, treatment 2; III, treatment 3.1, 163 K; 2, 323 K; 3, after O_2 admission at 323 K; ρ is wafer density (mg/cm^2).

ions caused by the loss of oxygen in the vicinity of extended defects (*15–17*).

For supported catalysts, the Cu^{2+} type centers could not be localized only on the surface of CuO phase. This conclusion is supported by the lower intensity of this band for the samples containing CuO phases—Cu(20) and Cu(27) (see Figs. 5 and 6). Moreover, for the Cu–Al–O system there is a correlation between the number of Cu^{2+} ions registered by ESR and the relative concentration of the centers characterized by the 2180–2190 cm^{-1} bands (Fig. 7, Tables 3 and 6). These data suggest that, for the supported catalysts, centers of this type correspond to isolated and weakly interacting Cu^{2+} ions on the surface of γ-alumina.

2150–2160 cm^{-1}

Bands in this spectral region were observed on interaction of CO with hydroxyl groups on the surface of γ-Al_2O_3 (*24*) (Table 4, No. 4). Analogous phenomena (a decrease in band intensity in the 3650–3800 cm^{-1} region and the appearance of broad absorption in the ca. 3600 cm^{-1} region after admission of CO at 163 K) were also observed in our experiments. However, after vacuum and CO treatments at 623 K, the concentration of OH groups did not increase while the intensity of the 2160 cm^{-1} band enhanced or passed through a maximum (Cu(7)–Cu(27)), as is evident from Fig. 5.

Because the 2150–2160 cm^{-1} band is stable only at 163 K, it may be attributed to CO adsorbed on Cu^{2+} ions. This absorption band appears at higher CO converage (pressures) (CO less strongly bound) than the 2180–2190 cm^{-1} band assigned to CO adsorbed on isolated Cu^{2+} (Fig. 8). It is known that for the Me^{n+} (Cu^{2+}, Al^{3+}, Co^{2+}, Ni^{2+}, etc.) a decrease in the effective charge of the adsorption center leads to a simultaneous decrease in bond strength and ν_{CO} (*19, 20*). Therefore, we may conclude that these centers of CO adsorption (ν_{CO} ca. 2160 cm^{-1}) differ from those of the isolated ions by having a less positive effective charge. Most likely, ions are clustered, and there is a second coordination sphere that contains not only Al^{3+} ions but also cations with lower charge (Cu^{2+}, Cu^{1+}). For samples reduced by CO as well as complexes of adsorbed CO with low thermostability, the 2155–2165 cm^{-1} band, which is stable at room temperature, can be observed (Table 4, No. 7). According to (*30*) it is assigned to isolated Cu^{1+} ions in the support surface.

Estimation of the density of adsorption centers (Cu^{2+} ions) has revealed that their surface coverage for the samples with low copper content is in the range 10–50% of monolayer, which indicates their considerable abundance in accordance with the ESR data.

2080–2110 cm^{-1}

For the sample reduced in CO at 623 K this band is attributed to CO adsorbed on large particles of metallic copper (*30*) (Fig. 5). After the sample was heated to 323 K, a

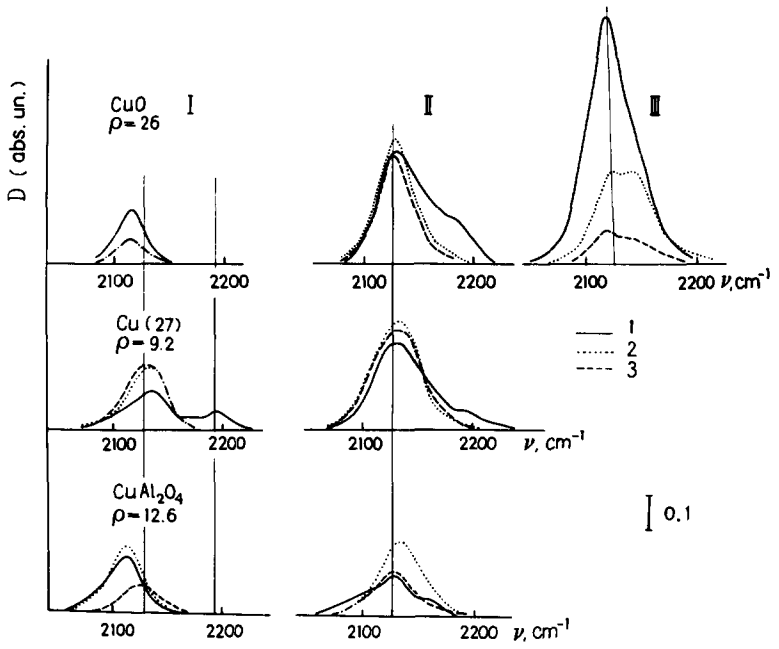

FIG. 6. Infrared spectra of CO adsorbed on CuO, Cu(27), $CuAl_2O_4$ samples. The designations are the same as those in Fig. 5.

strong decrease of this band intensity was found to be a result of CO desorption (the heat of CO adsorption on metallic copper is ca. 40 kJ/Mole (*31*)). The same effect was observed after O_2 addition, leading to the oxidation of Cu^0. In the latter case a simultaneous increase in the intensity of the 2120–2140 cm^{-1} band corresponding to Cu^{1+}–CO complexes (*14, 32*) was observed (Cu(20), Fig. 5).

One could be surprised at the appearance of the low-frequency (2100–2110 cm^{-1}) shoulder for nearly all the oxidized Cu–Al–O samples, even at 163 K. The concentration of the corresponding centers is increased after vaccum treatment, thus indicating their reduced character (Cu^0 or Cu^{1+}) (*32*). According to electron microscopy data, vacuum treatment of Cu(3.5) and Cu(7) leads to the appearanace of large clusters. Therefore, we suggest that the centers of CO adsorption forming complexes with ν_{CO} ca. 2080–2110 cm^{-1} may be attributed to the three-dimensional clusters found earlier for CuO/MgO and CuO/γ-Al_2O_3 systems (Table 4, No. 10).

For bulk aluminate, the appearance of these easily reduced clusters seems to be associated with considerable surface enrichment with copper ions (*6*). Indeed, the highest Cu/Al ratio for $CuAl_2O_4$ (Table 2) and reconstruction of its surface (Fig. 3) are in accordance with this supposition.

One reason for the appearance of Cu^0 centers on oxidized samples may be the easy removal of oxygen from these clusters by carbon monoxide even at 163 K, which indicates their high reactivity.

In a number of cases, the introduction of oxygen to the IR cell at 323 K was accompanied by an increase in the intensity of the 2120–2140 cm^{-1} band corresponding to Cu^{1+} centers (see Fig. 5, Cu(7), treatments 1,2). The only explanation for this is oxidation of centers that are more reduced than Cu^{1+} (i.e., Cu^0), which is typical of type 2 clusters (*14*). The addition of oxygen at room temperature has also led to an increase in the intensity of bands of carbonate–carboxylate complexes due to the oxidation of adsorbed or gaseous CO. Therefore, CO catalytic oxidation proceeds even at room

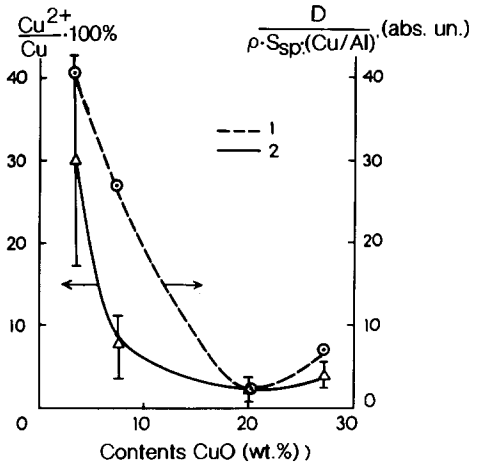

FIG. 7. Correlation between the percentage of isolated Cu^{2+} ions detected by ESR and the intensity of 2180–2190 cm^{-1} absorption bands normalized to the surface concentration of copper. (ρ, wafer density; S_{sp}, specific surface; Cu/Al, the surface ratio of Cu/Al by XPS data).

temperature. This can probably be explained by a low energy of adsorbed oxygen bonding for type 2 clusters (*14*). According to our estimation, the number of Cu^0 centers for oxidized samples is highest for $CuAl_2O_4$ (ca. 20% of monolayer); for Cu(27) it is close to ca. 5% of monolayer.

2110–2140 cm^{-1}

According to (*30*), bands in this spectral region correspond to CO adsorbed on Cu^{1+} ions. Because the same bands were found for bulk CuO, the question arises whether the centers for all samples could be localized on copper oxide microcrystals.

First, note an essential difference in the behavior of these bands for oxidized samples warmed from 163 to 323 K (for bulk CuO there was a decrease in the intensity; for Cu–Al–O samples including those without CuO phase, i.e., Cu(7), Cu(3.5), and there was usually an increase in the intensity (Figs. 5 and 6)). This increase in intensity is easily explained by the reduction of the sample surface with CO and therefore by the increase in the number of Cu^{1+} ions. Moreover, for the CuO phase the complexes with this ν_{CO} were found to exhibit considerably lower stability. During CO evacuation at 323 K for CuO this band disappeared at ca. 10^{-1} Torr, and for the Cu(3.5) and Cu(20) samples these bands were detectable even at 10^{-3} Torr.

A fuller understanding of the nature of Cu^{1+} centers may be gained from correlative analysis of the trends in variations of different band intensities passing from one sample to another (Fig. 9). For samples in the oxidized state (with the exception of Cu(20)) the intensity of the 2110–2140 cm^{-1} band varies in parallel with the intensity of the 2080–2110 cm^{-1} band. The latter is assigned to CO adsorbed on Cu^0 centers in type 2 clusters. Therefore, it seems likely that for oxidized samples the Cu^{1+} centers are localized mainly on the surface of these clusters. The presence of the easily reducible part of the active component for the initial Cu(3.5) and Cu(7) samples is supported by XPS data (see above). For the Cu(20) sample this correlation is not valid. It may be explained by ascribing the 2120–2140 cm^{-1} band of this sample mainly to Cu^{1+} centers on the surface of highly dispersed and defect CuO particles.

Because the centers of CO adsorption (Cu^{1+} ions) for bulk CuO are probably localized in the vicinity of the outlets of extended defects (twins and dislocations (*17*)), these defects being observed in CuO particles on the support, it was reasonable to expect the appearance of the same centers for the Cu(20) and Cu(27) samples. However, as mentioned above, the behavior and chemical properties of these centers for supported samples are somewhat different from those of the pure CuO phase. Our explanation of this phenomenon is a supposition about the modification of the supported CuO phase by Al ions. Indeed, a considerable dissolution of alumina in impregnating solutions was demonstrated earlier (*18*). Therefore, Al ions may be included in the supported CuO particles, most probably concentrated in the vicinity of extended defects (*35*). The concentration of Al ions in the vicinity of twin boundaries was confirmed by EDX spectral analysis (Fig. 10; the spectrum was obtained

TABLE 4
The Proposed Nature of CO Adsorption Centers

No.	Structure of the adsorption center	Location of adsorption center	Samples	ν_{CO} (cm^{-1})
1	Al—O—$\underline{Al^{3+}}$—O—Al	Al^{3+} in γ-Al_2O_3	Cu(3.5)–Cu(27)	2180–2190
2	Al—O—$\underline{Cu^{2+}}$—O—Al	Isolated and weakly associated Cu^{2+}	Cu(3.5)–Cu(27)	
3	Cu^{2+}—O—$\underline{Cu^{2+}}$—O—Cu^{2+}	Cu^{2+} ions in CuO	CuO	
4	OH O—Al—O	Hydroxyls of γ-Al_2O_3	Cu(3.5)–Cu(27)	2155–2165
5	Cu^{1+}—O—$\underline{Cu^{2+}}$—O—Cu^{1+}	Cu^{2+} ions near	CuO	
6	Cu^{1+}—O—$\underline{Cu^{2+}}$—O—Al	Cu^{1+}	All except CuO	
7	Al—O—$\underline{Cu^{1+}}$—O—Al	Isolated and weakly associated Cu^{1+}	Cu(3.5)–Cu(27)	
8	Cu—O—$\underline{Cu^{1+}}$—O—Cu Cu—O O—Cu	Cu^{1+} ions of supported CuO phase	Cu(20) Cu(27)	2110–2140
9	Cu—O—$\underline{Cu^{1+}}$—O—Cu Al^{3+}—O O—Al^{3+}	Two-dimensional Cu—O clusters on the surface of γ-Al_2O_3	All Cu—Al—O samples	
10	$\underline{Cu^{1+}}$ O Cu	Three-dimensional clusters on γ-Al_2O_3	All Cu—Al—O samples	2080–2110
11	$\underline{Cu^0}$ Cu Cu	Three-dimensional clusters on γ-Al_2O_3		
12	Cu—$\underline{Cu^0}$—Cu Cu Cu	Cu^0 phase on γ-Al_2O_3	All except Cu(3.5) Cu(7)	

Note. Underline indicates the center of CO adsorption. The proposed structures characterize only the qualitative peculiarities of its nearest coordination sphere, enabling one to explain the spectral and chemical properties.

from CuO isolated from γ-alumina particles).

After vacuum treatment at 623 K the intensities of the 2110–2140 cm^{-1} and 2160 cm^{-1} bands change in a similar manner (Fig. 9, curves 2, 4). This enables us to suppose that for vacuum-treated samples, Cu^{1+} centers are associated mainly with type 1 clusters with a bridging oxygen (*12–14*). Some deviation in this correlation for the Cu(20) sample may be explained as above by a contribution from Cu^{1+} centers on the surface of CuO particles. The estimations have shown that for vacuum-treated samples in general there are more Cu^{1+} centers than Cu^0 centers, reaching a maximum ca. 20% of the monolayer $CuAl_2O_4$ and ca. 10% of monolayer for Cu(7).

The classification of various centers is given in Table 4. A predominant portion of the active component for Cu(3.5) is in the form of isolated ions and type 1 clusters. On the surface of Cu(7) there are also many large type 2 clusters. The surface of $CuAl_2O_4$ is covered mainly with clusters. For Cu(20) the appearance of the CuO phase is accompanied by a decrease in the number of type 2 clusters in comparison with Cu(7). The greater density of clusters for Cu(27) may be due to the different preparation methods (*18*). On the surface of Cu(20) and Cu(27) there are also type 1 clusters and isolated ions.

Infrared Spectra of Spent Catalysts

The original spectra of adsorbed CO for spent catalysts are given in Fig. 11. The variations in characteristic band intensity of

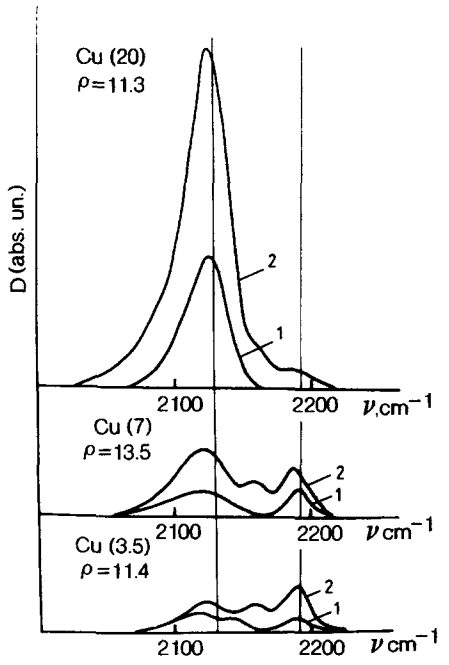

FIG. 8. Pressure dependence of infrared spectra of adsorbed CO: 1, 10^{-2} Torr; 2, 20 Torr.

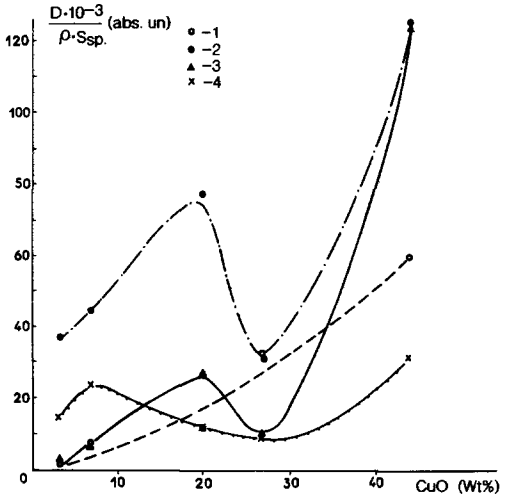

FIG. 9. Intensities of characteristic absorption bands versus copper content: 1, 2080–2110 cm^{-1} (323 K, treatment 1); 2, 2110–2140 cm^{-1} (163 K, treatment 2); 3, 2110–2140 cm^{-1} (323 K, treatment 1); 4, 2150–2160 cm^{-1} (163 K, treatment 2).

adsorbed CO, which may be attributed to definite types of copper–oxygen structures, are given in Table 5.

In general, it is necessary to emphasize the noticeable change in the behavior of CO bonds for spent samples compared with that of fresh samples (Figs. 5, 6, 11). For Cu(7) the overall decline in intensity is accompanied by a loss in the ability of the band intensity to increase after the sample is warmed from 163 to 323 K; i.e., it is related to the decrease in the sample reactivity (see above). For spent Cu(27) the overall band intensity at 163 K is somehat increased but the loss of reducibility on heating is pronounced; for Cu(20) there is an increase in reactivity and a reduction in intensity at 163 K. These facts may be interpreted as indications of an increase in the concentration of type 2 clusters for Cu(20) and a decrease for Cu(7) and Cu(27) specimens. The intensity of the 2080–2110 cm^{-1} band changes in accordance with this supposition (see Table 5).

According to our electron microscopic data and to results of previous work (*27*) for Cu(7) and Cu(27) samples the destruction of the regions with high copper enrichment is accompanied by the formation of more or less perfect particles of CuO and aluminate possessing low reactivity. The decrease in the intensity of low-frequency bands and sample reactivity for these specimens may be explained by the destruction of the above-mentioned metastable reactive structures. For the Cu(20) sample (Table 5) this

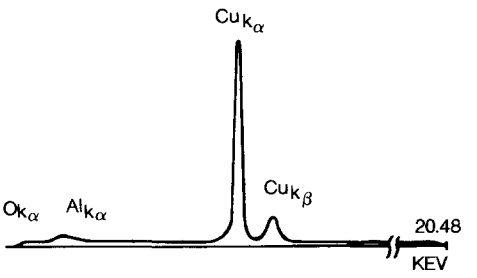

FIG. 10. EDX spectrum obtained from the twinning region of the CuO particle supported on γ-Al_2O_3. Accelerating potential, 100 kV.

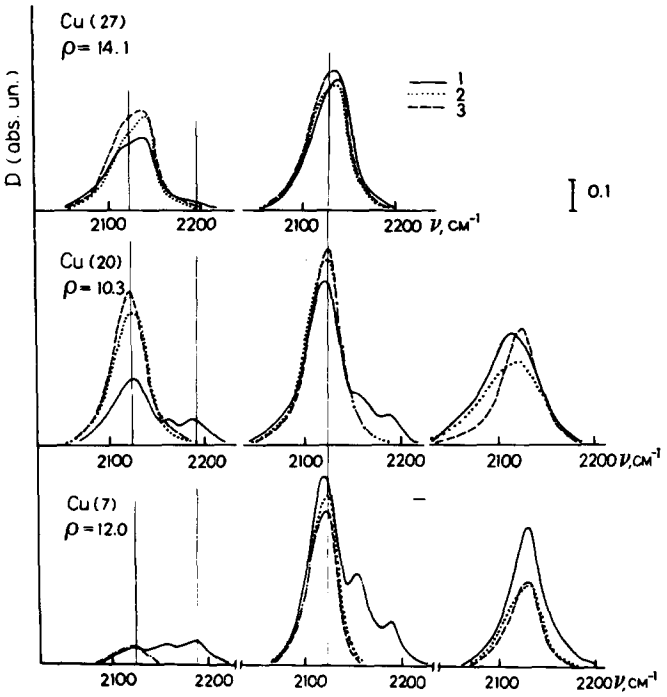

FIG. 11. Infrared spectra of CO adsorbed on spent samples. The designations are the same as those in Fig. 5.

scheme is not valid because there is an increase in reactivity and in the 2080–2110 cm^{-1} band intensity (Fig. 11). This may be an indication of the disproportionation of type 1 clusters under the influence of reaction media on large structures (CuO particles and type 2 clusters) and isolated ions. This supposition is in agreement with the fact that despite the formation of additional defect particles of the CuO phase, the relative occurrence of type 2 clusters for the spent Cu(20) sample remains practically unchanged in contrast to the situation for spent Cu(7) and Cu(27) specimens in which the concentration of isolated ions increases (Tables 3 and 5).

In addition to variations in the density of clusters, it is necessary to emphasize the considerable modification of the properties of CuO particles in the catalysts. For fresh Cu(20) the reduction in CO at 623 K (Fig. 5) has caused practically complete disappearance of the high-frequency bands due to the conversion of all copper components to the

TABLE 5

Relative Intensities ($I_{spent}/I_{initial}$) for Characteristic Absorption Bands of Spent Catalysts

Sample	2080–2110 cm^{-1}, 323 K, treatment 1	2130–2140 cm^{-1} 323 K, treatment 2	2190 cm^{-1} 163 K, treatment 1
Cu(7)	0.5	0.52	0.2
Cu(20)	1.7	0.71	10
Cu(27)	0.12	0.33	0.1

TABLE 6

The Enthalpies of Oxygen Adsorption (kJ/mole) Calculated by the Interacting Bond Method

Structure	Center of adsorption	Face	
		(110)	(100)
$CuAl_2O_4$	Cu in octahedra	106	—
	Epitaxial layer of CuO without Cu–Cu bond formation	140	—
γ-Al_2O_3	Cu in octahedra	123	—
	Epitaxial layer of CuO without Cu–Cu bond formation		
	MO form	164	130
	M_2O form	288	—
	Three-dimensional CuO with NaCl structure and Cu–Cu bond formation (M_5O form)	—	18

metallic state. For the spent Cu(20) sample reduced in CO, a considerable portion of the high-frequency bands corresponding to Cu^{2+} and Cu^{1+} ions has been preserved. These results are in agreement with corresponding XPS data (see above). This decrease in sample reactivity may be related to the annealing of the extended defects in CuO particles (*17*). Indeed, for spent Cu(20) after treatment 1 the intensity of the 2110–2140 cm^{-1} band at 163 K attributed to Cu^{1+} centers on the surface of CuO particles is considerably lower than that of the fresh sample (cf. Figs. 5 and 11). The absence of detectable absorption bands at ν_{CO} 2100 cm^{-1} after reduction of the spent Cu(7) sample in CO at 573 K also indicates a low reactivity of the CuO phase in this specimen.

DISCUSSION

1. Bonding Energy of Oxygen and Reactivity of Various Copper–Oxygen Species

To discover whether the bonding energy of oxygen in various Cu–O structures can determine their reactivity, the semiempirical interacting bond method (*34*) has been used. The calculation results are given in Table 6. It was found that the heat of oxygen adsorption on isolated copper atoms in the octahedral environment is ca. 110–170 kJ/mole, which indicates its moderate reactivity. Two-bonded oxygen in flat clusters of copper ions should be less reactive: its heat of adsorption is about 300 kJ/mole. Oxygen from type 1 clusters can probably be removed only via surface diffusion to easily reducing type 2 clusters.

As a model for the latter clusters, the structure that might form when CuO is supported on the (100) face of γ-Al_2O_3 was analyzed. It seems reasonable to suggest that in supported layers of CuO the oxygen atoms continue the oxygen network of spinel with the same parameters. For geometric reasons the copper atoms should be located in octahedral sites, thus forming a NaCl-type structure. For bulk CuO this structure is thermodynamically unfavorable: the calculated heat of CuO (tenorite) atomization is ca. 63 kJ/mole higher. However, the interaction with the support that firmly fixes and oxygen sublattice could stabilize this structure. The heat of oxygen adsorption for this cluster calculated with the supposition of Cu–Cu bond formation after oxygen removal is ca. 22 kJ/mole.

According to estimations (Table 6), the surface oxygen in these clusters should have a low bonding energy and high reactivity. However, analysis has revealed that with an increase in cluster should reduction the energy of oxygen bonding also increases, thus preventing complete transition to the

Cu^0 state. Therefore, the reduction of type 2 clusters should give rise to Cu^0 as well as Cu^{1+} centers. Type 2 clusters with an NaCl-type structure may appear in the vicinity of support surface defects such as steps and pits. The high density of steps for bulk $CuAl_2O_4$ correlates with the highest concentration of type 2 clusters for this specimen.

2. *The Nature of Catalyst Aging in Reaction Media*

It should be noted that the reactivity of the CuO phase on the support decreased considerably in reaction media. The newly formed CuO particles in spent Cu(7) also possessed low reactivity. From the TEM and IR spectroscopic data obtained in this work, one may conclude that the origin of these phenomena is associated with a decrease in the density of extended defects. Therefore, this process, which was previously observed for bulk CuO (*17*), has manifested itself for the supported phase, too.

The other principal aspect of the influence of reaction media is the destruction of a metastable heterogeneous surface solid solution. This process can be traced most clearly for Cu(7) and Cu(20) samples that had a relatively short contact with the reaction media. It leads to the formation of new particles of the CuO phase, with large clusters serving as nuclei of crystallization. The subsequent growth of the particles of CuO can proceed only at the expense of the destruction of type 1 clusters. By necessity, it leads to an increase in the number of isolated copper ions that was observed for spent Cu(20). Evidently, the destruction of type 1 clusters proceeds through the intermediate formation of three-dimensional clusters (see above) with their subsequent rearrangement into perfect CuO particles. One reason for the decline in the catalyst activity under the influence of reaction media may be the result of this reconstruction of three-dimensional clusters. As in the annealing of metastable extended defects in CuO particles, the reaction medium facilitates the transition of these active structures to more stable but less reactive ones.

Finally, the aging of copper–alumina catalysts is accompanied by crystallization and accumulation of bulk aluminate, as was manifested for Cu(27) after 1.5 years of use. It should be emphasized that in the temperature range typical of detoxication reactors (673–683 K), this process occurs only in reaction media; calcination in air at these temperatures did not lead to any variation in the phase composition or activity of catalysts (*27*). It should be noted that bulk aluminate is not thermodynamically stable at temperatures below 843 K (*35*). The rate of formation and the stability of bulk aluminate increased considerably under slightly reducing conditions of reaction media when disordering of the CuO surface layer (by accumulation of point defects) and that of the support (by destruction of initial solid solution) take place. This process was most pronounced for Cu(27), which had been left the longest in reaction media (Table 1). As a result, the amount of CuO phase (*27*) was considerably reduced. Therefore, in reaction media after destruction of the initial metastable solid solution (a relatively fast process leading to an increase in amount of the CuO phase), the process of bulk aluminate formation was sufficiently slow that the bulk of the support could be restructured. In this case the driving force seems to be associated with the increase in entropy due to the formation of bulk solid solution.

Formation of bulk aluminate is accompanied by migration of copper ions to tetrahedral interstices, and this process is reflected in the decrease in the number of isolated ions detected by ESR (pairs of Cu_{Td}–Cu_{Oh} formed) (Table 3). A question naturally arises about the influence of the aluminate accumulation on the activity of catalysts. Indeed, for Cu(27) the accumulation of aluminate is accompanied by a decrease in the intensity of low-frequency bands (diminishing the number of three-dimensional clusters) and by a decrease in the reactivity. However, aluminate formation could be a

sideline process, whereas deactivation might be determined exclusively by annealing extended defects in CuO particles and restructuring large clusters. The last hypothesis is supported by the fact that the intensity of low-frequency bands for the stoichiometric bulk aluminate (Fig. 6) is higher than that for all other samples.

To explain this phenomenon, one should take into account that aluminate formed in Cu(27) is characterized by a lower overall copper content and Cu/Al ratio in the surface layer than the stoichiometric $CuAl_2O_4$ annealed in air at 583 K (Table 2). This should lead to a less pronounced tendency for large cluster segregation under comparable conditions. Moreover, due to the thinner aluminate particles on the support, the exposure of (001) faces that are most favorable for the segregation of reactive clusters is considerably lower, which should also lead to low reactivity.

Therefore, the formation of nonstoichiometric aluminate (with deficiency in copper) could also be responsible for the decrease in activity after aging in reaction media.

CONCLUSIONS

The nature of surface centers of supported $CuO/\gamma\text{-}Al_2O_3$ catalysts active in the reactions of catalytic oxidations has been elucidated by microstructural investigations combined with spectroscopic methods and theoretical calculations. The main results are:

1. The precursor species for the most reactive sites were metastable three-dimensional oxide clusters easily reduced with carbon monoxide to Cu^0.

2. A number of centers more or less differing by their coordination, which could easily be reduced to the Cu^{1+} state, have been observed. They are associated with: (a) extended defects (twins, dislocations) in CuO particles, (b) two- and three-dimensional Cu–O clusters, and (c) isolated copper ions in the surface layer of the γ-alumina support.

3. The catalyst deactivation in reaction media seems to be a result of the annealing of extended defects in the CuO phase and destruction of three-dimensional clusters with the formation of bulk aluminate deficient in copper and/or CuO particles.

ACKNOWLEDGMENTS

We are thankful to Dr. Yu. Barabanenkov (Institute of Crystallography, Moscow) for providing EDX spectroscopy data.

REFERENCES

1. Thomas, C. L. "Catalytic Processes and Proven Catalysts." Academic Press, New York, 1970.
2. Hodges, L. "Environmental Pollution." Holt, Rinehart & Winston, New York, 1972.
3. Behara, R., *Appl. Catal.* **16,** 15 (1985).
4. Hierl, R., Knozinger, H., and Urbach, H. P., *J. Catal.* **69,** 475 (1981).
5. Strohmeier, B., Leiden, D. E., Field, R. S., and Hercules, D. M. *J. Catal.* **94,** 514 (1985).
6. Ertl, G., Hierl, R., Knozinger, H., Thiele, N., and Urbach, H. P. *Appl. Surf. Sci.* **5,** 49 (1980).
7. Barber, M., Sharpe, P. K., and Vickerman, J. C., *J. Catal.* **41,** 240 (1976).
8. Lumbeck, H., and Voitlander, J., *J. Catal.* **132,** 117 (1969).
9. Friedman, R. B., Freeman, J. J., and Lyttle, FV. W., *J. Catal.* **55,** 10 (1978).
10. Lo Jacono, M., and Schiavello, M., *in* "Preparation of Catalysts" (B. Delmon, P. A. Jacobs, and G. Poncelet, Eds.), p. 473, Elsevier, Amsterdam, 1976.
11. Lo Jacono, M., Cimino, A., and Inversi, M., *J. Catal.* **76,** 320 (1982).
12. Lokhov, Yu. A., Morozov, L. N., Davydov, A. A., and Kostrov, V. V., *Kinet. Katal.* **21,** 1295 (1980). [in Russian]
13. Lokhov, Yu. F., Musil, Z., and Davydov, A. A., *Kinet. Katal.* **20,** 256 (1979). [in Russian]
14. Lokhov, Yu. A., Zailkovskii, V. I., and Solomennikov, A. A., *Kinet. Katal.* **23,** 418 (1982). [in Russian]
15. Lokhov, Yu. A., Sadykov, V. A., Tikhov, S. F., and Popovskii, V. V., *Kinet. Katal.* **26,** 177 (1985). [in Russian]
16. Kryukova, G. N., Zaikovskii, V. I., Sadykov, V. A., Tikhov, S. F., Popovskii, V. V., and Bulgakov, N. N., *J. Solid State Chem.* **74,** 191 (1988).
17. Sadykov, V. A., Tikhov, S. F., Kryukova, G. N., Bulgakov, N. N., Popovskii, V. V., and Kolomiichuk, V. N., *J. Solid State Chem.* **74,** 200 (1988).
18. Starostina, T. G., Pivovarova, I. V., Tsyrulnikov, P. G., Popovskii, V. V., Kuznetsov, O. N., Plyasova, L. M., and Ketchik, S. V., *Z. Prikl. Khim.* **53,** 933 (1980). [in Russian]

19. Soltanov, R. I., Paukshtis, E. A., and Yurchenko, E. N., *Kinet. Katal.* **23,** 164 (1982). [in Russian]
20. Soltanov, R. I., Paukshtis, E. A., Yurchenko, E. N., Dadashev, B. A., Mamedov, S. E., and Gasymov, B. A., *Kinet. Katal.* **25,** 729 (1984). [in Russian]
21. Seanor, D. A., and Amberg, C. H., *J. Phys. Chem.* **42,** 2967 (1965).
22. Arendarskii, D. A., Paukshtis, E. A., Ismagilov, Z. R., and Yurchenko, E. N., *React Kinet. Catal. Lett.* **25,** 729 (1984).
23. de Jong, K. P., Geus, J. W., and Joziasse, *J. Appl. Surf. Sci.* **6,** 273 (1980).
24. Bazhin, N. M., and Tsvetkov, Yu. D. "Hyperfine Structure of the ESR Centers of Free Radicals." Novosibirsk State University, Novosibirsk, 1971.
25. Wagner, C. D., Davis, L. E., Zeller, M. V., Taylor, J. A. Raymond, R. H., and Gale, L. H., *Surf. Interface Anal.* **3,** 211 (1981).
26. Smith, D. J., Bursill, L. A., and Jefferson, D. A., *Surf. Sci.* **175,** 673 (1986).
27. Starostina, T. G., Tsyrulnikov, P. G., Pivovarova, I. V., Popovskii, V. V. Plyasova, L. M., Ketchik, S. V., Zaikovskii, V. I., and Noskova, S. P., *Zh. Prikl. Khim.* **54,** 2452 (1981).
28. Okamoto, Y., Fukino, K., Imanaka, T., and Teranishi, S., *J. Phys. Chem.* **87,** 3740 (1983).
29. Sexton, B. A., Smith, T. D., and Sanders, J. V., *J. Electron Spectrosc. Relat. Phenom.* **35,** 27 (1985).
30. Lokhov, Yu. A., and Davydov, A. A., *Kinet. Katal.* **20,** 1498 (1979). [in Russian]
31. Rapp, H., and Pritchard, J., *Surf. Sci.* **53,** 241 (1975).
32. Salomatin, G. I., Lafer, L. I., and Yakerson, V. I., *Izv. Akad. Nauk SSSR, Ser. Khim. Nauk* **7,** 1445 (1979). [in Russian]
33. Friedel, J., "Le Dislocations." Gauthiers-Villar, Paris, 1956.
34. Bulgakov, N. N., Borisov, Yu. A., and Popovskii, V. V., *Kinet. Katal.* **14,** 468 (1973). [in Russian]
35. Jacob, K. T., and Alcock, C. B., *J. Am. Ceram. Soc.* **57,** 192 (1975).